Rocksalt versus layered ordering in double perovskites: A case study with La_2CuSnO_6 and La_2CuIrO_6

Kartik Samanta and Tanusri Saha-Dasgupta*

Department of Condensed Matter Physics and Material Science, S. N. Bose National Centre for Basic Sciences, Kolkata 700106, India

(Received 24 March 2017; published 1 June 2017)

The nature of ordering of B and B′ transition metal ions in double perovskite compounds of general composition $A_2BB'O_6$ is an important topic, since the physical properties crucially depend on it. In the present study, considering the specific cases of La_2CuSnO_6 and La_2CuIrO_6, we carry out first-principles calculations with an aim to obtain microscopic understanding on this issue. Our study reveals the presence of Jahn-Teller distorted B ion, like Cu^{2+} helps in band energy stabilization of the layered ordering over the rocksalt ordering. However, introduction of magnetism may reverse this trend, especially in the presence of a second magnetic ion at B′ site, which may introduce a strong superexchange path involving B-O-B′, as found in the case of La_2CuIrO_6. We further find the spin-orbit coupling at Ir site drives the La_2CuIrO_6 compound to be a spin-orbit assisted Mott insulator.

DOI: 10.1103/PhysRevB.95.235102

I. INTRODUCTION

Research on perovskite oxides with general formula ABO_3 formed by corner-shared transition metal (TM) based BO_6 octahedra that contain rare-earth/alkaline-earth A cation in 12-coordinate sites is an ever-growing area. This has attracted the attention of condensed matter physicists, solid-state chemists, and material scientists for ages [1]. From the perspective of materials designing, it is desirable to have the flexibility in choice of components. In this context, double perovskite family with general formula $A_2BB'O_6$, where prime indicates the possibility of a choice of different TM ion other than B, provides additional degrees of freedom over the normal perovskite family. Double perovskites have been reported to show diverse electrical and magnetic properties [2] and considered as potential candidates for multiferroicity [3], spintronics [4], magnetocapacitive behavior [5,6], and magneto-optic device materials [7]. The arrangement of B and B′ cations, however, is an extremely important issue, as most properties crucially depend on this. Apart from random arrangement of B and B′ cations, which leads to disordered perovskite structure with formula $A(B_{1/2}B'_{1/2})O_3$, there are three different arrangements that are possible, namely columnar, layered, and rocksalt, as shown in Fig. 1.

To date, most attempts on synthesizing double perovskites resulted into either random disordered or in order rocksalt arrangement of B and B′ cations, with a very few rare examples [8] of double perovskites with layered ordering of B and B′. The general consensus or rule of thumb is that a large difference of valence (at least two or more) and difference in ionic radius of B and B′ are helpful for driving the ordering. It was further pointed out that having two different geometries of BO_6 and $B'O_6$ octahedra, for example, the combination of an Jahn-Teller (JT) distorted B ion, like Cu^{2+} and an undistorted B′ ion, further stabilizes the layered ordering over the rocksalt ordering. Following this idea, layer-ordered compound, La_2CuSnO_6, was first synthesized by Anderson *et al.* [9]. Later layer-ordered double perovskites R_2CuSnO_6 with smaller rare-earth cations, R = Nd/Pr/Sm and La_2CuZnO_6, were synthesized using high pressure [10]. While the presence of Jahn-Teller distorted Cu^{2+} ion appears to be necessary for stabilization of layered ordering of B and B′ sites, it is however not sufficient. For example, La_2CuTiO_6 shows random arrangement [11], while La_2CuIrO_6 or La_2CuMnO_6 shows rocksalt ordering of B and B′ ions [12]. Cationic sizes have been held responsible for such behavior [10]. The microscopic understanding though, to the best of our knowledge, has not been achieved.

In the present study, we would like to address the above issue within the framework of first-principles density functional theory (DFT) calculations, by considering the examples of La_2CuSnO_6 (LCSO) and La_2CuIrO_6 (LCIO). In particular, we study the relative stability of LCIO and LCSO compounds between the layered and rocksalt ordering, considering (a) the band structure effect, (b) the effect of magnetism, and (c) effect of spin-orbit coupling (SOC). We note, for LCIO, Ir is in 4+ valence state, which has been discussed heavily in the context of the competing effect of spin-orbit coupling and electron-electron correlation [13].

Our study shows that consideration of only band structure effect stabilizes both LCSO and LCIO in the layered structure, dominated by the two-dimensional (2D) nearest-neighbor Cu-Cu hopping. Introduction of magnetic interaction though does not affect the structural stability of LCSO; its effect is found to be dramatic for LCIO, making rocksalt ordering favorable compared to layered. This reversing in relative structural stability is found to be driven by the strong Cu-Ir superexchange interaction. The magnetism-driven stability of rocksalt ordering over layered ordering in LCIO is found to hold well also in the presence of SOC effect at Ir site. We further found LCIO is a strong spin-orbit driven Mott insulator, in agreement with the findings of recent literature [14].

II. COMPUTATIONAL DETAILS

The DFT calculations have been carried out with the choice of three different basis sets: (a) the plane-wave based basis as implemented in the Vienna *ab initio* Simulation Package (VASP) [15], (b) the full potential linear augmented plane wave (FLAPW) basis as implemented in WIEN2K code [16],

*t.sahadasgupta@gmail.com

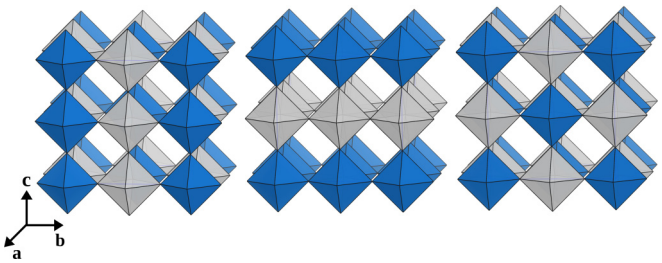

FIG. 1. Schematic representation of three different ordering of BO_6 and $B'O_6$ octahedra, possible in a double perovskite structure. The BO_6 and $B'O_6$ octahedra are marked with two different colors. From left to right, the figure shows the columnar, layered, and rocksalt ordering.

(c) the muffin-tin orbital (MTO) based linear muffin-tin orbital (LMTO) [17] method, and the Nth order MTO method, namely, NMTO method [18] as implemented in the STUTTGART code. The consistency of the calculations in three different basis sets is cross checked in terms of density of states, and band structure calculations.

The structural optimization as well as total energy calculations have been carried out using the plane wave basis [15] with projector-augmented wave (PAW) potentials [19]. During the structural optimization in the plane wave basis, the lattice parameters as well as atomic positions have been relaxed maintaining the symmetry of the crystal. The positions of the atoms were relaxed towards equilibrium until the Hellman-Feynman forces become less than 0.001 eV/Å. A plane-wave cutoff of 560 eV and Monkhorst-Pack k-point mesh of $6 \times 4 \times 6$ for $P\bar{1}$ symmetry and $4 \times 6 \times 6$ for $P2_1/m$ symmetry were found to provide a good convergence of the total energy.

The total energy calculations of different structures as well as the calculations including spin-orbit coupling have been carried out in all electron full potential methods of LAPW. For self-consistent calculations in the LAPW basis the number of k points in the irreducible BZ is chosen to be 168 for $P\bar{1}$ symmetry and 147 for $P2_1/m$ symmetry. The commonly used criterion relating the plane wave and angular momentum cutoff, $l_{\max} = R_{\mathrm{MT}} \times K_{\max}$, was chosen to be 7.0, where R_{MT} is the smallest MT sphere radius and $K_{\max}$ is the plane wave cutoff for the basis. The chosen MT radii for La, Cu, Sn, Ir, and O were 2.42 Å, 2.02 Å, 2.08 Å, 2.09 Å, and 1.71 Å, respectively. The SOC was dealt through a second variational method.

The construction of low energy Hamiltonian in first-principles derived Wannier function basis was achieved through NMTO-downfolding technique starting from a full DFT band structure [18]. The NMTO calculations have been carried out with the potential borrowed from self-consistent LMTO calculation [17]. The real space representation of the NMTO-downfolded Hamiltonian, $H_{TB} = \sum_{ij} t_{ij}^{mm'}(C_{i,m}^{\dagger} C_{j,m'} + \mathrm{H.c.})$, in the Wannier function basis gives the on site ($t_{ii}^{mm'}$) and various hopping integrals ($t_{ij}^{mm'}$), where m and m' are nondownfolded orbitals at sites i and j, and $C_{i,m}^{\dagger}(C_{i,m})$ are electron creation (annihilation) operators.

The exchange-correlation functional for calculations in three different basis sets was chosen to be that of generalized gradient approximation (GGA) implemented following the Perdew-Burke-Ernzerhof (PBE) prescription [19]. To account

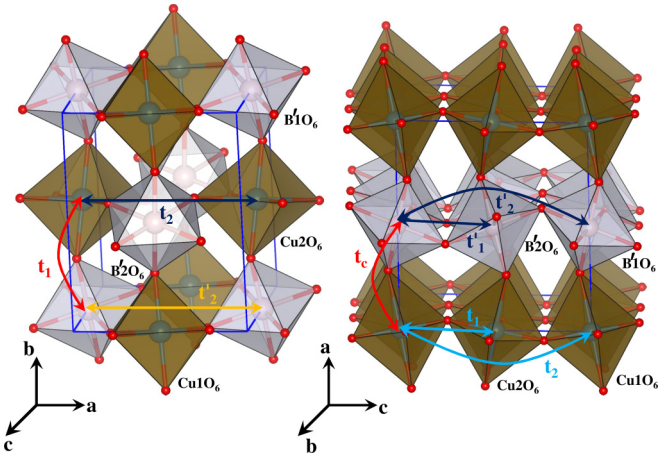

FIG. 2. Crystal structures of $P\bar{1}$ space group (left panel) and $P2_1/m$ space group (right panel), showing the rocksalt and layered ordering of CuO_6 (brown/dark gray) and $B'O_6$ (light gray, $B' = Sn/Ir$) octahedra, respectively. Two inequivalent CuO_6 ($Cu1O_6$ and $Cu2O_6$) and $B'O_6$ ($B'1O_6$ and $B'2O_6$) octahedra are labeled in both the structures. The La ions sitting in the void created by the corner-shared octahedra are not shown for clarity. The dominant hopping paths, t_1, t_2, t_2' for rocksalt ordered structure and t_1, t_2, t_1', t_2', t_c for layer ordered structure have been also marked.

for the effect of strong electron-electron correlation at magnetic ions Cu and Ir, the missing correlation beyond GGA was taken into account through supplemented Hubbard U (GGA+U) calculation [20]. For the U values we chose the typical values for $3d$ and $5d$ transition metal oxides. The results reported in the following have been obtained for U(Cu) = 4 eV and U(Ir) = 1 eV, with Hund's coupling, J_H, of 0.8 eV. We have also checked the validity of our results by varying the U value by $+/-2$ eV at Cu site, and by $+/-1.0$ eV at Ir site. The trend in the results was found to remain unchanged.

III. CRYSTAL STRUCTURES

The crystal structure of LCIO was originally predicted to be a four formula unit monoclinic $P2_1/n$ space group [21] with cell dimension, $\sqrt{2}a_p \times \sqrt{2}a_p \times 2a_p$, indicating rocksalt ordering of Cu and Ir ions, with a_p being the lattice parameter for the cubic perovskite structure. However, the very recent neutron diffraction as well as powder XRD measurement [22] on polycrystalline sample confirms the low-symmetry $P\bar{1}$ space group with two formula unit cell. This crystal structure is derived from distorted rocksalt structure with alternating CuO_6 and IrO_6 octahedra along three crystallographic axes. Both CuO_6 and IrO_6 octahedra are distorted, with larger distortion of CuO_6 octahedra compared to IrO_6, in conformity with stronger JT activity of e_g-derived states of Cu, compared to t_{2g}-derived states of Ir [23]. The low symmetry of triclinic space group results into two inequivalent octahedral sites of both Cu and Ir giving rise to two different types of alternating layers along the crystallographic b axis, as shown in the left panel of Fig. 2.

The experimentally measured crystal structure of LCSO is reported to be of monoclinic $P2_1/m$ space group with four formula units having two inequivalent Cu atoms, two inequivalent Sn atoms, and four inequivalent La sites. The

cell size is of dimension $2a_p \times 2a_p \times 2a_p$. As shown in the right panel of Fig. 2, the structure consists of three kinds of 2D layers, CuO_2, SnO_2, and LaO. The CuO_2 and SnO_2 planes are strongly buckled with tilting of JT distorted CuO_6 octahedra and that of SnO_6 octahedra. The La cations are displaced towards the CuO_2 layer.

To study the relative structural stability of the rocksalt and layered ordering, we considered both LCIO and LCSO in their respective ground state structures with specific ordering type (rocksalt or layered), as well as in the assumed structures with the other kind of ordering. While for layered ordering, the only reported space group is the monoclinic $P2_1/m$ space group, for the rocksalt ordering several different space groups have been reported for different double perovskites, namely cubic ($Fm-3m$), tetragonal ($I2/m$), rhombohedral ($R\bar{3}$), and monoclinic ($P2_1/n$) [8]. While the cubic rocksalt contains no tilt of the TM octahedra, tetragonal, and rhombohedral as well as monoclinic structures are characterized with octahedral tilts, the tilt pattern being different between different structures. In Glazer notation [24], tetragonal structure shows the $a^0b^-b^-$ tilt pattern, while rhombohedral and monoclinic structures are found to show $a^-a^-a^-$ and $a^-b^-b^-$ tilt patterns, respectively. The tolerance factor (t) of both LCIO and LCSO being less than 1 (0.945 for LCIO and 0.930 for LCSO [25]), the structures with octahedral tilts are favored compared to cubic untilted structure. Generally, for $t < 0.97$, the crystal structure is expected to be monoclinic [26]. One would thus expect both LCIO and LCSO to form in monoclinic symmetry. In agreement with this expectation, among the tetragonal ($I2/m$), rhombohedral ($R\bar{3}$), and monoclinic ($P2_1/n$) structures, the monoclinic structure is found to be lowest in energy for the assumed rocksalt ordering for both LCSO and LCIO compounds. We compared the energetics for recently suggested $P\bar{1}$ space group with that of $P2_1/n$ structure, and found them to be comparable, with $P\bar{1}$ structure slightly lower in energy compared to $P2_1/n$, the energy difference being $\approx$2 meV/f.u. for LCIO and $\approx$5 meV/f.u. for LCSO. In the following, all analyses have been presented considering $P2_1/m$ and $P\bar{1}$. However, a very similar trend has been obtained considering $P2_1/n$ symmetry for the rocksalt ordering.

To be specific, we considered LCIO in the experimentally measured symmetry of $P\bar{1}$ and in the $P2_1/m$ symmetry of layered ordered structure. Similarly, we considered LCSO in the experimentally measured symmetry of $P2_1/m$ and in the $P\bar{1}$ symmetry of rocksalt-type ordered structure. As mentioned above, for each symmetry, the lattice parameters as well as the internal coordinates were relaxed completely. Since the choice of exchange correlation can have an influence on the optimized lattice parameters and thus on internal coordinates, we compared our optimized structures of $P\bar{1}$ symmetry for LCIO and $P2_1/m$ symmetry for LCSO, for which experimental results are available [9,22]. The DFT optimized crystal structure shows 1%–2% larger volume compared to the experimentally determined volume. Its influence on octahedral rotations and JT distortions are found to be marginal (less than 2° for rotation and less than 0.05 Å for distortion). The volume difference of LCIO or LCSO in the two symmetries turns out to be less than 1%. The trend obtained from enthalpy turned out to be the same as that from energy. In the following, we have reported the structural stability in terms of energetics.

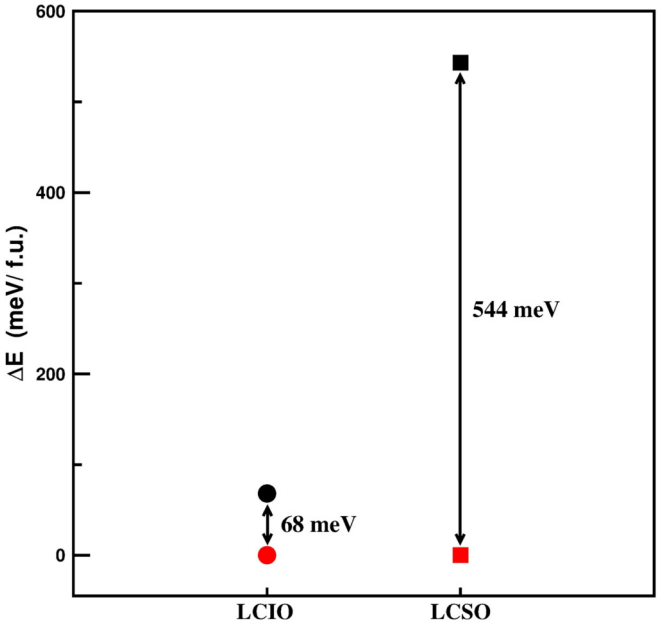

FIG. 3. Non-spin-polarized total energy difference (ΔE) of LCIO (circles) and LCSO (squares) between the optimized $P\bar{1}$ symmetry structure (black symbols) and $P2_1/m$ symmetry (red/dark gray symbols) structure. The positive value of ΔE indicates stability of $P2_1/m$ symmetry over $P\bar{1}$ symmetry.

IV. STRUCTURAL STABILITY

In order to find out the relative structural stability of LCIO and LCSO between the rocksalt and layered ordering of B and B′ sites, we first compared the total energies of the two compounds in two assumed symmetries, namely $P2_1/m$ and $P\bar{1}$, within the non-spin-polarized scheme of calculation. This is expected to take into account primarily the band structure effect, governing by the charge transfer and hopping interactions. Figure 3 shows the energetics, where $\Delta E = E_{\text{non}}(P\bar{1}) - E_{\text{non}}(P2_1/m)$, $E_{\text{non}}(P\bar{1})$ and $E_{\text{non}}(P2_1/m)$ being the energies of the optimized nonmagnetic $P\bar{1}$ symmetry structure and $P2_1/m$ symmetry structure, respectively. We found that, for both LCIO and LCSO, the $P2_1/m$ symmetry with layered ordering of B and B′ sites is favored compared to $P\bar{1}$ symmetry. We however found the energy gain in layer-ordered structure to be substantial for LCSO ($\approx$544 meV/f.u.), while it is about an order of magnitude smaller for LCIO ($\approx$68 meV/f.u.).

In the next stage, we incorporated the effect of magnetism. Apart from ferromagnetic (FM) structure with parallel alignment of all Cu and Ir spins, we considered three different antiferromagnetic (AFM) structures for LCIO, possible within the unit cell of $P2_1/m$ and $P\bar{1}$, namely AFM-A, AFM-C, and AFM-G. Similarly, apart from FM structure with parallel alignment of all Cu spins, we considered one and two different AFM structures for LCSO, namely AFM-A, and AFM-1D and AFM-2D, possible within the unit cell of $P\bar{1}$, and $P2_1/m$, respectively. Note that LCIO contains two magnetic ions, namely Cu and Ir, while LCSO contains a single magnetic ion, namely Cu. The considered magnetic structures are shown in Fig. S1 of the Supplemental Material (SM) [27]. Figure 4 shows the energetics within the

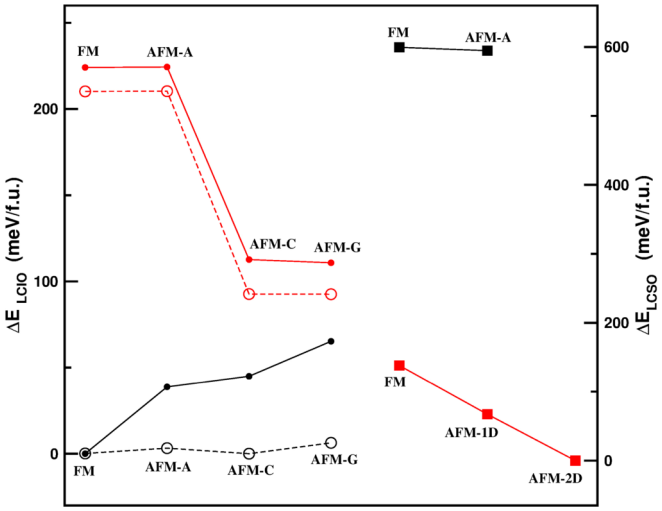

FIG. 4. Comparison of GGA+U total energy of LCIO (circles) and LCSO (squares) between the rocksalt and layer ordered structures, considering different magnetic structures. See SM [27] for the considered magnetic structures. Plotted are the total energy differences (ΔE) for the optimized $P2_1/m$ symmetry (red/dark gray symbols) structure and the $P\bar{1}$ symmetry structure (black symbols). See text for details. The positive value of ΔE for LCSO and LCIO indicates stability of $P2_1/m$ symmetry over $P\bar{1}$ symmetry, and of $P\bar{1}$ symmetry over $P2_1/m$ symmetry, respectively. The open symbols in case of LCIO represent results corresponding to GGA+U+SO calculations.

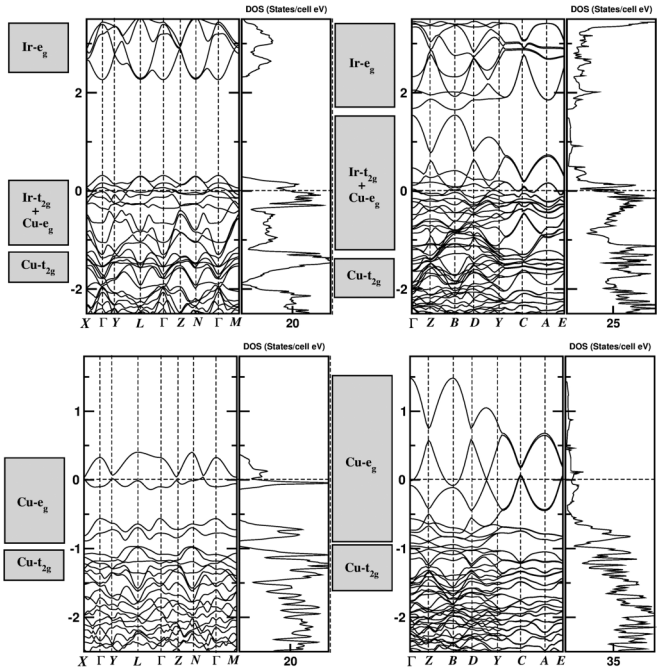

FIG. 5. Non-spin-polarized band structure and density of states of LCIO (upper panels) and LCSO (lower panels) in the rocksalt ordered $P\bar{1}$ symmetry (left panels), and layer ordered $P2_1/m$ symmetry (right panels). Band structure is plotted along the high-symmetry k points of the triclinic (for $P\bar{1}$ symmetry) BZ and the monoclinic (for $P2_1/m$ symmetry) BZ. The zero of the energy is set at the calculated values of Fermi energy (E_F). The dominant orbital characters of the states are shown by side.

GGA+U scheme of calculation, where for LCIO, $\Delta E = E - E_{\mathrm{FM}}(P\bar{1})$, with $E_{\mathrm{FM}}(P\bar{1})$ and E being the energy of the optimized $P\bar{1}$ symmetry structure in FM phase and that of optimized $P\bar{1}$ or $P2_1/m$ symmetry structure in different magnetic structures, respectively. Similarly for LCSO, $\Delta E = E - E_{\mathrm{AFM-2D}}(P2_1/m)$, with $E_{\mathrm{AFM-2D}}(P2_1/m)$ and E being the energy of the optimized $P2_1/m$ symmetry structure in AFM-2D phase and that of optimized $P\bar{1}$ or $P2_1/m$ symmetry structure in different magnetic structures, respectively.

Inclusion of supplemented U correction was found to be crucial to stabilize the magnetic moments at the Cu and Ir sites. The computed values of magnetic moments for LCIO at Cu and Ir sites are found to be about $0.5\,\mu_B$ and 0.4–$0.6\mu_B$, respectively, for choice of U(Cu) = 4 eV, U(Ir) = 1 eV, and $J_H = 0.8$ eV. The magnetic moment of Cu for LCSO is found to be about $0.6 - 0.7\,\mu_B$, for choice of U(Cu) = 4 eV and $J_H = 0.8$ eV. The computed magnetic moments are tabulated in SM [27]. Very interestingly, we found the magnetism helps stabilization of rocksalt ordering in the case of LCIO, irrespective of the considered magnetic structure. The lowest energy FM configuration in $P\bar{1}$ symmetry is found to be lower than the lowest energy AFM-G configuration in $P2_1/m$ symmetry by $\approx$110 meV/f.u. The effect of magnetism on structural stability of LCSO, on the other hand, turned out to be minimal. The layered ordering continued to remain favored for LCSO over the rocksalt ordering for all different magnetic arrangements. The lowest energy magnetic configuration of AFM-2D in layered $P2_1/m$ structure of LCSO is found to be stabler compared to lowest energy AFM-A magnetic configuration in rocksalt ordered $P\bar{1}$ structure of LCSO by $\approx$590 meV/f.u., in the same order as the nonmagnetic energy stabilization of 544 meV/f.u.

In order to check the effect of SOC, which is expected to be important for LCIO, we repeated the calculation of energetics including spin-orbit coupling. The effect of SOC is found to be marginal for LCSO, for which the orbital moment at Cu site is nearly quenched. The most dominant effect of SOC is found to be on Ir site of LCIO, with a calculated orbital moment of $\approx 0.3\mu_B$. The calculation of magnetocrystalline anisotropy energy showed the Ir moments to lie in plane, in agreement with experimental observation [22]. Even with inclusion of SOC, the rocksalt ordered LCIO is found to be systematically stabler compared to layered ordering for all chosen magnetic configurations. The inclusion of SOC, however, made the energetics of different magnetic configurations highly competitive, with AFM-C having Ir spins aligned in plane as the lowest energy magnetic configuration among the chosen magnetic configurations within the unit cell of $P\bar{1}$.

V. MICROSCOPIC ANALYSIS

In order to gain a microscopic understanding of the energetics, presented above, we analyze the electronic structure of LCSO and LCIO.

Figure 5 shows the plot of non-spin-polarized electronic structure of LCIO and LCSO in the rocksalt ordered $P\bar{1}$ symmetry and layer ordered $P2_1/m$ symmetry. The crystal field splitting due to the octahedral coordination of oxygen

atoms surrounding B and B′ ions results in board grouping of d states into states of t_{2g} and e_g symmetries. The JT distorted CuO_6 octahedra are elongated for LCSO both in layer ordered $P2_1/m$ symmetry and in rocksalt ordered $P\bar{1}$ symmetry, while for LCIO the CuO_6 octahedra are elongated in $P2_1/m$ symmetry and compressed in $P\bar{1}$ symmetry. This leads to splitting of Cu e_g states, with $d_{x^2-y^2}$ lying above $d_{3z^2-r^2}$ in the case of elongated octahedra, and the reverse for the compressed octahedra, with choice of local coordinate system having z axis pointing along Cu to apical oxygen bond. The states crossing E_F in LCSO are thus composed of Cu $d_{x^2-y^2}$ states corresponding to d^9 configuration of Cu^{2+} and filled shell configuration of Sn^{4+}. The states crossing E_F in LCIO, on the other hand, are composed of Cu $d_{x^2-y^2}$ (for $P2_1/m$ symmetry) or Cu $d_{3z^2-r^2}$ (for $P\bar{1}$ symmetry) and the t_{2g} states of Ir^{4+}, as seen in top panels of Fig. 5. For LCSO, there are two Cu $d_{x^2-y^2}$ bands crossing E_F for $P\bar{1}$ symmetry, contributed by two Cu ions present in the unit cell, while for $P2_1/m$ symmetry there are four such bands contributed by four Cu ions present in the unit cell (cf. bottom panels of Fig. 5). We notice a significant narrowing, by about 75%, of the bandwidth of the low-energy bands in the rocksalt ordered structure, compared to layer ordered structure. In comparison, considering the contribution of Cu $d_{3z^2-r^2}$ or Cu $d_{x^2-y^2}$, and Ir t_{2g} bands in LCIO, this narrowing of bandwidth in rocksalt ordered structure compared to layer ordered structure is only about 40%.

In order to quantify the above-described band structure effect, we further carried out NMTO-downfolding calculations. For this purpose, we constructed the low-energy Hamiltonian in effective Cu $d_{x^2-y^2}$ Wannier function basis for LCSO in the ground state $P2_1/m$ symmetry as well as in the assumed $P\bar{1}$ symmetry, starting from the non-spin-polarized band structure of LCSO, and integrating out all the degrees of freedom other than Cu $d_{x^2-y^2}$. Similar exercise was carried out for LCIO in its ground state $P\bar{1}$ symmetry, and the assumed $P2_1/m$ symmetry in the effective Cu $d_{3z^2-r^2}/d_{x^2-y^2}$–Ir t_{2g} Wannier basis, starting from the non-spin-polarized band structure of LCIO, and integrating out all the degrees of freedom other than Cu $d_{3z^2-r^2}/d_{x^2-y^2}$ and Ir t_{2g} states. The choice of the active (nondownfolded) orbitals are decided by the dominant orbital characters close to Fermi energy. The real space representation of these low-energy Hamiltonians, as described in Sec. II, provides the information of effective Cu-Cu, Cu-Ir, and Ir-Ir hopping interactions. The dominant hopping paths for the rocksalt ordering turned out to be t_1 connecting the nearest neighbor Cu and B′, t_2 connecting second nearest-neighbor Cu-Cu, and t_2' connecting second nearest-neighbor B′−B′ (cf. Fig. 2). For LCSO with filled shell Sn^{4+} only t_2 is significant. Similarly the dominant hopping paths for the layered ordering turned out to be t_1, the in-plane nearest-neighbor Cu-Cu hopping, t_2, the in-plane second nearest-neighbor Cu-Cu hopping, t_1', the in-plane nearest-neighbor B′−B′ hopping, t_2', the in-plane second nearest-neighbor B′−B′ hopping, and t_c, the out-of-plane Cu-B′ hopping (cf. Fig. 2). For LCSO with filled shell Sn^{4+}, Sn-Sn, and Cu-Sn hoppings (t_1', t_2', and t_c) are neglected. The calculated values of dominant hopping integrals are listed in Table I for LCSO and LCIO in both the structures.

Focusing on the case of LCSO, we find dominant Cu $d_{x^2-y^2}$–Cu $d_{x^2-y^2}$ hopping connecting the in-plane nearest neighbor Cu ions in the layered structure is more than an order of magnitude larger compared to the second nearest neighbor Cu $d_{x^2-y^2}$–Cu $d_{x^2-y^2}$ hopping for the rocksalt structure. This causes a large band energy gain of the layered structure of LCSO over the rocksalt structure, supporting the conclusion from band structure and energetics. Considering the case of LCIO, the combined effect of large Cu $d_{x^2-y^2}$–Cu $d_{x^2-y^2}$ hopping and large Ir t_{2g}–Ir t_{2g} hopping in layered structure turns out to be stronger when weighed against the Cu $d_{3z^2-r^2}$–Ir t_{2g} hopping in rocksalt structure. This in turn explains the stabilization of the layered structure over the rocksalt for the nonmagnetic LCIO, though the stabilization is weaker compared to that of LCSO.

In the next stage, we performed massive downfolding, where we kept only Cu $d_{x^2-y^2}$ or $d_{3z^2-r^2}$ active and integrated the rest. The Wannier functions of the corresponding effective orbitals are plotted in Fig. 6 for LCSO and LCIO in two different symmetry structures, namely $P2_1/m$ and $P\bar{1}$. The central part of the Wannier functions, positioned at Cu site, are shaped according to $d_{x^2-y^2}$ or to $d_{3z^2-r^2}$ symmetry. The tails of the Wannier functions are shaped according to integrated out O-p or Ir-t_{2g} states. While all the four Wannier functions show significantly weight at O sites, indicating the presence of strong antibonding Cu-O covalency, the Wannier function for LCIO in $P\bar{1}$ symmetry with rocksalt ordering of Cu and Ir sites, additionally shows appreciable weight at neighboring Ir, suggestive of a well defined Cu-O-Ir superexchange path. We notice, for LCIO in layered structure, the weight at the out-of-plane Ir site is negligible, due to $d_{x^2-y^2}$ symmetry of the active Cu orbital which shows little overlap with the out-of-plane Ir t_{2g} orbitals. The superexchange driven Cu-Ir magnetism therefore contributes to a large extent in lowering the energy of the rocksalt ordering compared to layered ordering.

VI. ELECTRONIC STRUCTURE OF MAGNETIC LCSO AND LCIO

A. La_2CuSnO_6

Considering the different magnetic structures, total energy calculations show the antiferromagnetic ordering of in plane Cu^{2+} spins gives the lowest energy magnetic configuration in the ground state $P2_1/m$ symmetry. This is in conformity with the prediction on magnetic structure based on temperature dependent susceptibility measurement [9], which assigns antiferromagnetic coupling of Cu moments. The board maxima in temperature dependent susceptibility curve signals low dimensionality, namely the 2D ordering of Cu spins. Figure 7 shows the plot of GGA+U density of states and band structure for layer-ordered $P2_1/m$ LCSO with 2D antiferromagnetic ordering of Cu spins. As is seen from the plot, like in case of nonmagnetic electronic structure, the Cu d levels, apart from $d_{x^2-y^2}$ are fully filled. The low energy electronic structure though are qualitatively different between the nonmagnetic situation and the magnetic one. Upon introduction of 2D antiferromagnetism and correlation effect within the framework of GGA+U, the majority spin Cu $d_{x^2-y^2}$ becomes completely filled and the minority spin Cu $d_{x^2-y^2}$ becomes completely empty, thereby resulting into an semiconducting solution, as opposed to the metallic solution

TABLE I. Calculated hopping integrals (in eV), as given by NMTO-downfolding calculations, for LCSO and LCIO in $P\bar{1}$ and $P2_1/m$ symmetry. For each hopping type, the number of neighbors N_n and hopping integrals for one of the representative connecting vector is listed. The hopping integrals for other connecting vectors corresponding to same hopping type should be obtained by consideration of symmetry operations. The large hopping integrals are marked in bold.

Compound	Connecting vector hopping int.	N_n	Atoms		$d_{x^2-y^2}$			
LCSO ($P\bar{1}$)	[−0.775 0.004 0.087] t_2	4	Cu1-Cu1/ Cu2-Cu2	$d_{x^2-y^2}$	−0.021			
LCSO ($P2_1/m$)	[0.000 0.000 −0.501] t_1	4	Cu1-Cu1/Cu2	$d_{x^2-y^2}$	**0.330**			
	[0.000 0.000 1.001] t_2	4	Cu1-Cu1/ Cu2-Cu2	$d_{x^2-y^2}$	−0.015			
LCIO ($P\bar{1}$)	[0.000 0.500 0.000] t_1	6	Cu1-Ir2/Ir1		$d_{3z^2-r^2}$	d_{xy} **−0.116**	d_{yz} −0.014	d_{xz} −0.130
	[−0.778 0.001 0.016] t_2	4	Cu1-Cu1/ Cu2-Cu2		$d_{3z^2-r^2}$	$d_{3z^2-r^2}$ 0.017		
	[−0.778 0.001 0.016] t_2'	4	Ir1-Ir1/ Ir2-Ir2		d_{xy} d_{yz} d_{xz}	d_{xy} −0.002 0.008 −0.025	d_{yz} 0.008 0.006 −0.060	d_{xz} −0.025 −0.060 0.016
LCIO ($P2_1/m$)	[0.563 0.000 −0.024] t_c	2	Cu1-Ir1/ Cu2-Ir2		$d_{x^2-y^2}$	d_{xy} 0.005	d_{yz} 0.007	d_{xz} −0.008
	[0.000 0.000 0.502] t_1	4	Cu1-Cu1/Cu2		$d_{x^2-y^2}$	$d_{x^2-y^2}$ **−0.326**		
	[0.000 0.000 1.005] t_2	4	Cu1-Cu1/ Cu2-Cu2		$d_{x^2-y^2}$	−0.013		
	[0.000 0.000 0.502] t_1'	4	Ir1-Ir1/Ir2		d_{xy} d_{yz} d_{xz}	d_{xy} −0.029 **−0.102** **0.252**	d_{yz} −0.001 −0.045 −0.061	d_{xz} 0.009 −0.013 0.021
	[0.000 0.000 1.005] t_2'	4	Ir1-Ir1/ Ir2-Ir2		d_{xy} d_{yz} d_{xz}	−0.003 −0.002 −0.002	−0.002 −0.018 −0.033	−0.002 −0.033 −0.034

for the nonmagnetic case. This semiconducting nature is in agreement with the conductivity measurement [9].

B. La_2CuIrO_6

Ir^{4+} oxides have been discussed heavily in literature due to the interplay between strong SOC driven physics, and Coulomb correlation effect [28]. Due to the large crystal field splitting of 5*d* Ir, the Ir^{4+} ion with d^5 configuration stabilizes in low-spin state with one hole in the t_{2g} manifold. Switching on the spin-orbit coupling, the t_{2g} bands split into $j_{\text{eff}} = 1/2$ doublet and $j_{\text{eff}} = 3/2$ quartet states. The $j_{\text{eff}} = 3/2$ states being lower in energy compared to $j_{\text{eff}} = 1/2$ states become fully filled for d^5 configuration of Ir. Thus $j_{\text{eff}} = 1/2$ band which lie higher in energy compared to $j_{\text{eff}} = 3/2$ becomes half-filled. This makes the situation comparable to conventional Mott insulators, in which Coulomb correlation may drive the insulating state for half-filled bands of appropriate bandwidth. The width of $j_{\text{eff}} = 1/2$ bands turns to be small, so that even a modest U value is found to open the gap, as discussed initially in the context of layered Sr_2IrO_4 [13]. The $j_{\text{eff}} = 1/2$ Mott picture is found to largely hold well also for double perovskites having nonmagnetic B ion and magnetic B′ ion like La_2ZnIrO_6 or La_2MgIrO_6, though a finite mixing between $j_{\text{eff}} = 1/2$ and $j_{\text{eff}} = 3/2$ states was pointed out [29]. We find the same to be true for La_2CuIrO_6, where both B and B′ ions are magnetic. This is in conformity with a recent paper [14].

Figure 8 shows the band structure and density of states of LCIO within the calculation scheme of GGA+U and GGA+U+SOC, in the AFM-C magnetic structure. While the non-spin-polarized electronic structure leads to metallic solution (cf. Fig. 5), introduction of magnetism and the missing correlation within the scheme of GGA+U makes it nearly insulating (cf. left panel in Fig. 8). The introduction of moderately large U value together with spin splitting at Cu site makes the Cu $d_{3z^2-r^2}$ completely filled in the majority spin channel and empty in the minority spin, the states in two spin channel being separated by a large energy separation of ≈3 eV. The Ir t_{2g} states span an energy range of ≈2 eV around E_F, which are 5/6th filled. The finite distortion of the IrO_6 octahedra, on the other hand, causes splitting within Ir t_{2g} states, which leads to a dip in the density of states at E_F but

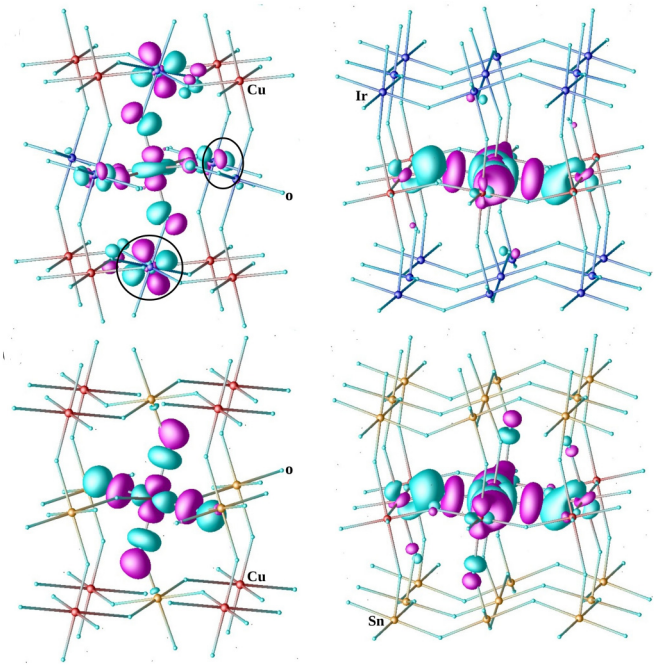

FIG. 6. Wannier functions of effective $d_{x^2-y^2}$ or $d_{3z^2-r^2}$ orbitals plotted for LCIO (upper panels) and LCSO (lower panels) for the rocksalt (left panels) and layer ordered (right panels) structures. Plotted are the constant value surfaces, with positive and negative lobes of the wave functions colored differently. The significant weight sitting at the Ir site for the rocksalt ordered LCIO has been encircled.

cannot open up a clear gap. Increase of U value within 0.5 to 1.0 eV does not change the scenario. However, inclusion of SOC (cf. right panel in Fig. 8) opens up a clear gap at E_F of $\approx$0.3 eV in agreement with findings of a recent study [14]. We find that introduction of SOC together with supplemented U effect splits the Ir t_{2g} manifold into groups of eight, two, and two bands. The projection to $j_{\text{eff}} = 1/2$ and $j_{\text{eff}} = 3/2$

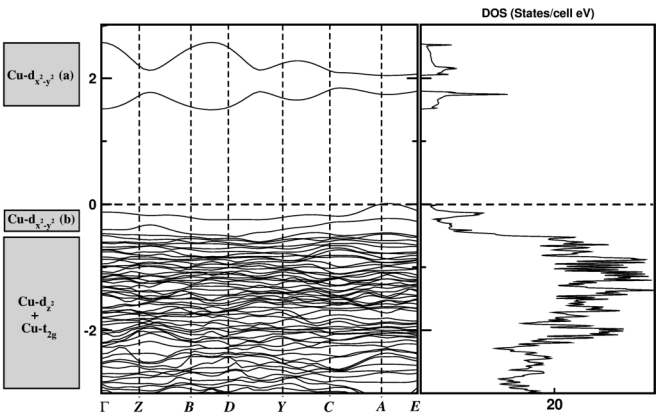

FIG. 7. Band structure and density of states of LCSO in magnetically ordered ground state of AFM-2D in layer ordered $P2_1/m$ symmetry. Band structure is plotted along the high-symmetry k points of the monoclinic BZ. The zero of the energy is set at the calculated values of E_F. The dominant orbital characters of the states are shown by side, with Cu $d_{x^2-y^2}$ (a)/(b) denoting the minority/majority spin bands.

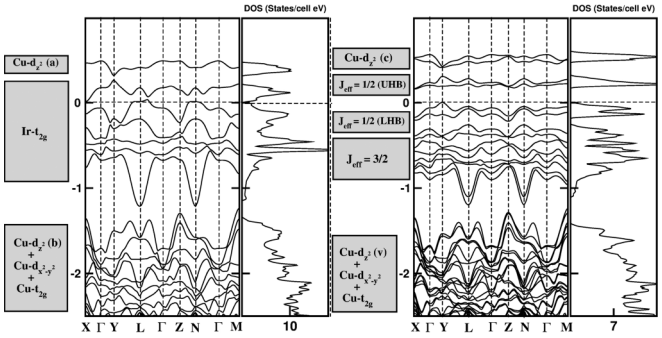

FIG. 8. Band structure and density of states of LCIO in magnetically ordered state of AFM-C in rocksalt ordered $P\bar{1}$ symmetry within GGA+U (left panel) and GGA+U+SOC (right panel) scheme of calculations. Band structure is plotted along the high-symmetry k points of the triclinic BZ. The zero of the energy is set at the calculated values of E_F. The dominant orbital characters of the states are shown by side. Cu d_{z^2} (a)/(b) denotes the minority/majority spin bands, while Cu d_{z^2} (c)/(v) denotes the UHB and LHB bands of Cu $d_{3z^2-r^2}$.

states leads us to conclude that the group lowest in energy among these are formed by $j_{\text{eff}} = 3/2$ bands, each Ir ion in the unit cell contributing four, while the following two groups are contributed by four $j_{\text{eff}} = 1/2$ bands arising out of two Ir ions in the unit cell, which get split into lower Hubbard band (LHB) and upper Hubbard band (UHB) due to the correlation effect. This in turn confirms LCIO to be a $j_{\text{eff}} = 1/2$ Mott insulator.

The spin configuration of LCIO has been recently examined by analysis of the low-temperature neutron diffraction data [22]. Based on that analysis the magnetic structure has been proposed to be that of collinear AFM spin arrangement in every ac plane (plane containing Cu1-Ir1 or Cu2-Ir2) and mutually orthogonal spin orientations in neighboring planes, as shown in the SM [27]. The realization of this magnetic structure requires a $2 \times 1 \times 2$ supercell of the $P\bar{1}$ triclinic cell. We computed the energy of this magnetic structure, and compared with the lowest energy magnetic structure realized within the unit cell of $P\bar{1}$, i.e., AFM-C. The former is found to be lower in energy by about 15 meV/f.u. The calculated density of states assuming this magnetic arrangement (see SM [27]) shows similar features as shown in the right panel of Fig. 7, with a SOC assisted Mott gap.

VII. SUMMARY AND DISCUSSIONS

In this study we have employed first-principles DFT calculations to gain microscopic understanding on the issue of B-cation arrangements in double perovskites. While most of the B-site ordered $A_2BB'O_6$ double perovskites are reported to exhibit ordering of B and B′ alternating along all three directions, the so-called rocksalt ordering, there exists a few of the compounds which show alternating of B and B′ cations only along one direction, the so-called layered ordering. Arguments have been given in terms of geometric considerations for this behavior [8], but here we discuss the underlying electronic mechanism.

Considering the specific cases of LCSO and LCIO, we find that it is the band structure effect given by large in-plane nearest-neighbor Cu $d_{x^2-y^2}$–Cu $d_{x^2-y^2}$ hopping that favors the

layered ordering over the rocksalt ordering. We note Cu^{2+} is in d^9 configuration with $d_{x^2-y^2}$ as the only partially filled orbital. In this respect, one would expect having a strong JT distorted ion at B site, which favors large in-plane hopping, would be a good candidate for layer ordering. This narrows down the choice to e_g based systems which lead to directed $pd\sigma$ bonds as well as produce a strong JT effect. Other than Cu^{2+} one of the possibilities could be Ni^{3+} with d^7 configuration [8]. However, Ni^{3+} in the context of nickelate perovskites [30] has been shown to be ideally behaving as $d^8\underline{L}$, where $\underline{L}$ is a ligand hole, which shows tendency towards charge disproportionation to $(d^8)(d^8\underline{L}^2)$, thereby avoiding the strong JT effect. This might explain why all the layer-ordered double perovskite compounds synthesized to date are Cu^{2+} based.

In order to maintain the band structure driven stability of the layer-ordered structure over rocksalt ordered structure, the choice of the second TM ion at B′ site should be chosen keeping in mind the effect of magnetism. While the strong in-plane nearest-neighbor B-B hopping favors ordering of B and B′ ions in layers over nearest-neighbor B-B′ arrangement as in rocksalt structure, this effect can be downplayed by the magnetism if B′ site has a magnetic ion as rigorously proved for the case of LCIO in the present study. In order to strengthen the validity of our conclusion, we have further carried out calculations on La_2CuMnO_6 (LCMO) compound. The details of the results can be found in the SM [27]. We found that following our prediction, while in the absence of magnetism the layered ordering is favored over rocksalt, turning on magnetism reverses the stability, making rocksalt favored over layered, in conformity with experimental observation [10]. Unfortunately only the disordered phase of the La_2CuTiO_6 compound exists [10], prohibiting theoretical study of cation ordering in this compound as this requires the knowledge of ordered crystal symmetry. However, if they can be made to order there exists a good possibility that they will form in layer ordered structure.

We further found that the effects of spin-orbit coupling keep the above described scenario unperturbed, though they play an important role in describing the ground state electronic structure. We hope that our findings will shed more light on the problem of cation ordering in double perovskites.

ACKNOWLEDGMENTS

K.S. and T.S.D. thank Department of Science and Technology, India for the support through Thematic Unit of Excellence. The authors thank S. Baidya and P. Sanyal for some of the initial calculations and fruitful discussions.

[1] S.-W. Cheong, Nat. Mater. **6**, 927 (2007).
[2] J. B. Philipp, P. Majewski, L. Alff, A. Erb, R. Gross, T. Graf, M. S. Brandt, J. Simon, T. Walther, W. Mader, D. Topwal, and D. D. Sarma, Phys. Rev. B **68**, 144431 (2003).
[3] M. Azuma *et al.*, J. Am. Chem. Soc. **127**, 8889 (2005).
[4] K.-I. Kobayashi, T. Kimura, H. Sawada, K. Terakura, and Y. Tokura, Nature (London) **395**, 677 (1998).
[5] N. S. Rogado, J. Li, A. W. Sleight, and M. A. Subramanian, Adv. Mater. **17**, 2225 (2005).
[6] H. Das, U. V. Waghmare, T. Saha-Dasgupta, and D. D. Sarma, Phys. Rev. Lett. **100**, 186402 (2008).
[7] H. Das, M. D. Raychaudhury, and T. Saha-Dasgupta, Appl. Phys. Lett. **92**, 201912 (2008).
[8] M. T. Anderson, K. B. Greenwood, G. A. Taylor, and K. R. Poeppelmeier, Prog. Solid State Chem. **22**, 197 (1993).
[9] M. T. Anderson and K. R. Poeppelmeier, J. Solid State Chem. **102**, 164 (1993).
[10] M. Azuma, S. Kaimori, and M. Takano, Chem. Mater. **10**, 3124 (1998).
[11] N. Ramadass, J. Gopalakrishnan, and M. V. C. J. Sastri, Inorg. Nucl. Chem. **40**, 1453 (1978).
[12] G. J. Blasse, Inorg. Nucl. Chem. **27**, 993 (1965).
[13] B. J. Kim, H. Jin, S. J. Moon, J. Y. Kim, B. G. Park, C. S. Leem, J. Yu, T. W. Noh, C. Kim, S. J. Oh, J. H. Park, V. Durairaj, G. Cao, and E. Rotenberg, Phys. Rev. Lett. **101**, 076402 (2008); B. J. Kim, H. Ohsumi, T. Komesu, S. Sakai, T. Morita, H. Takagi, and T. Arima, Science **323**, 1329 (2009).
[14] W. K. Zhu *et al.*, arXiv:1608.07763.
[15] G. Kresse and J. Furthmüller, Phys. Rev. B **54**, 11169 (1996).
[16] P. Blaha, K. Schwarz, G. K. H. Masden, D. Kvasnicka, and J. Luitz, in *Wien2k, An Augmented PlaneWave + Local Orbitals Program for Calculating Crystal Properties*, edited by K. Schwarz (Technische Universität Wien, Vienna, 2001).
[17] O. K. Andersen and O. Jepsen, Phys. Rev. Lett. **53**, 2571 (1984).
[18] O. K. Andersen and T. Saha-Dasgupta, Phys. Rev. B **62**, R16219 (2000).
[19] J. P. Perdew, K. Burke, and M. Ernzerhof, Phys. Rev. Lett. **77**, 3865 (1996).
[20] V. I. Anisimov, I. V. Solovyev, M. A. Korotin, M. T. Czyżyk, and G. A. Sawatzky, Phys. Rev. B **48**, 16929 (1993).
[21] A. V. Powell, J. G. Gore, and P. D. Battle, J. Alloys Compd. **201**, 73 (1993).
[22] K. Manna *et al.*, Phys. Rev. B **94**, 144437 (2016).
[23] P. G. Radaelli, New J. Phys. **7**, 53 (2005).
[24] P. M. Woodward, Acta Crystallogr. B **53**, 32 (1997).
[25] R. D. Shannon, Acta Crystallogr. A **32**, 751 (1976).
[26] D. Serrate, J. M. D. Teresa, and M. R. Ibarra, J. Phys.: Condens. Matter **19**, 023201 (2007).
[27] See Supplemental Material at http://link.aps.org/supplemental/10.1103/PhysRevB.95.235102 for the illustration of different magnetic structures, considered in the present study, the table of magnetic moments, the computed electronic structure considering the reported magnetic ordering of LCIO, and the results on La_2CuMnO_6.
[28] F. Wang and T. Senthil, Phys. Rev. Lett. **106**, 136402 (2011); X. Wan, A. M. Turner, A. Vishwanath, and S. Y. Savrasov, Phys. Rev. B **83**, 205101 (2011); G. Jackeli and G. Khaliullin, Phys. Rev. Lett. **102**, 017205 (2009).
[29] G. Cao, A. Subedi, S. Calder, J. Q. Yan, J. Yi, Z. Gai, L. Poudel, D. J. Singh, M. D. Lumsden, A. D. Christianson, B. C. Sales, and D. Mandrus, Phys. Rev. B **87**, 155136 (2013).
[30] S. Johnston, A. Mukherjee, I. Elfimov, M. Berciu, and G. A. Sawatzky, Phys. Rev. Lett. **112**, 106404 (2014).